Journal of Environment and Earth Science
ISSN 2224-3216 (Paper) ISSN 2225-0948 (Online)
Vol 2, No.11, 2012
www.iiste.org

Sub Pixel Classification Analysis for Hyperspectral Data (Hyperion) for Cairo Region, Egypt

Waleed Effat[1*] Osman Hegazy[2] Mohamed NourEldien[3]

1. Esri Northeast Africa, 4 El-Mathaf El-Zerai, Agouza, PO 12311, Giza, Egypt
2. Faculty of Computers and Information, Cairo University, PO Box 12613, Giza, Egypt
3. Faculty of Computers and Information, Cairo University, PO Box 12613, Giza, Egypt

* E-mail of the corresponding author: waleed.effat@gmail.com

Abstract

Traditional hard classifiers in remote sensing applications can label image pixels only with one class, so land cover (e.g. trees) can only be recorded as either present or absent. This approach might lead to inaccurate image classification and accordingly inaccurate land cover. The proposed analysis technique provides the relative abundance of surface materials and the context within a pixel that may be a potential solution to effectively identifying the land-cover distribution. This research is applied on the central region of Cairo using hyperspectral image data, which provides a large amount of spectral information. A spectral mixture analysis approach is used on Hyperion data (hyperspectral data) to produce abundance images representing the percentage of the existence of each material/land cover with a pixel. The uniqueness of this study comes from the fact that it is the first time Hyperion data has been used to extract land cover in Egypt.

Keywords: Spectral Mixture Analysis, Hyperspectral Data, Hyperion Data, Cairo, Egypt

1. Introduction

The regular image classification techniques are concerned with 'hard' pixel labeling. Most of the different classification schemas require that each individual pixel is given a single, unambiguous label. This objective is a justifiable one whenever regions of relatively homogeneous land cover occur in the image data. These regions should be large relative to the instantaneous field of view of the satellite sensor. In other instances the instantaneous field of view of the sensor may be too large for it to be safely assumed that a single pixel contains just a single land cover type. In many cases, a 1 km x 1 km pixel of AVHRR or ATSR image is unlikely to contain just one single cover type. Challenges might face any investigator whose concern is to classify each smaller pixel containing several cover types. If a conventional hard classifier is used, e.g. Maximum Likelihood, or parallelepiped, the result will have low classification accuracy. Many alternatives to the standard hard classification have been proposed. The method of mixture modeling starts from the explicit assumption that the characteristics of the observed pixels constitute mixtures of the characteristics of a small number of basic cover types (endmembers). The investigator can use a 'soft' classifier, which does not reach a definite conclusion in favor of one class or another. Instead, these soft classifiers present the user with a measure of the degree to which the given pixel belongs to some or all the candidate classes, and leaves to the investigator the decision as to the category into which the pixel should be placed.

In environmental application fields where visual information processing is involved, the use of spectral information is of great importance in performing some tasks. The trend for these applications is the use of spectral and spatial information in order to estimate and analyze certain phenomena. Hyperspectral images are a kind of multimodality, where spectral imaging is combined with digital image processing (Bearman, 2000; Leitner, 2003).

Hyperspectral technology is used to reconstruct spectral signatures of phenomena and to produce a spectral library for earth observation. Types of sensors that collect image data with hundreds of spectral bands include the NASA Jet Propulsion Laboratory (NASA/JPL) airborne visible/infrared imaging spectrometer (AVIRIS), the Naval Research Laboratory Hyperspectral Digital Imagery Collection Experiment (HYDICE) and Hyperion data (EO-1). Since the signatures of phenomena are represented in narrow bandwidth with fixed sample intervals, not all bands are useful for information extraction. Accordingly, determination of the informative bands in hyperspectral imagery needs to be considered for efficient representation of phenomena.

The objective of this paper is to produce classified images that represent the fractions of existence per pixel of each material within the area of the study.

The imagery data used in this study is Hyperion data (EO-1). Hyperion (Hyperspectral data), which covers a spectral range from 400 to 2500 nm and has 224 continuous channels with 10-nm bandwidth, is capable of distinguishing most of the terrestrial materials, including urban surface materials. The spatial resolution of Hyperion data is 30 meters from a 705 kilometer orbit (Goetz, 1992; Clark, 1999).

In the next section we will give a brief description of hyperspectral imagery versus multispectral data technology. The theory and concept will be presented in Section 3. In Section 4 we will demonstrate the material and methods used. The results are shown in Section 5, and finally conclusions are given in Section 6.

2. Hyperspectral imagery versus multispectral data

The use of hyperspectral data is a logical and obvious extension to multispectral data, which has been used extensively since the launch of the first LandSat system in 1972. In simple cases, such as the open ocean, algorithms used for analysis of multispectral data may be used to find endmembers, or explicit scene constituents, because the number of terrestrial objects is still less than the number of spectral bands measured. That is, it is possible to find endmembers, or use models, that can be used to determine the amount of a particular material in an unambiguous manner. This makes multispectral systems sufficient to attack problems where only limited information is present. However, as the complexity of the scene increases (such as the coastal ocean and urban land scenes), the number of scene objects increases beyond the number of bands being measured in a multispectral system. In these scenes, it is no longer possible to find endmembers that explicitly determine the presence of a particular constituent, but instead it is necessary to use additional techniques, such as clustering, to determine the different class populations, which portends ambiguity in the results. Over the last decade, the data produced by modern sensors have been increasing in quality and therefore information content, as ground sample distance (GSD) has been shrinking and signal-to-noise ratios (SNR) have been rising. Currently, it is possible for hyperspectral data to have SNR of well over 100:1 in the visible/near-infrared (VNIR) portion of the spectrum (outside the strong absorption features) at GSD sizes of 1–30 m and with spectral bandwidths of 5–10 nm. The exact SNR varies as a function of albedo, solar angles, atmospheric conditions, and measurement parameters (here, noise is considered to be the total of shot noise and "dark" sensor noise). As the quality of the data increases, the information content increases because of the ability of the systems to distinguish increasingly similar materials. (For example, a multispectral system can clearly determine the presence of vegetation, while an HSI can identify a particular species of plant.) The increase in information content portends the ability to extract additional useful information from the data. However, enhanced information content also makes it more difficult to find desired information and present it in a concise and meaningful way. A hyperspectral data set has so many bands that the data are, in most cases, spectrally over-sampled. In order to have a versatile multipurpose instrument, the hyperspectral approach is desirable.

3. Theory and Concept

Many methods have been used to determine the unmixing percentage located in each pixel in the satellite image, the most well-known of which is Linear Spectral Unmixing. In a linear mixed model it can be assumed that a single photon impinging upon a target on the Earth's surface is reflected into the field of view of the sensor without interacting with any ground surface object, then the totality of photons reflected from a single pixel area on the ground and intercepted by a sensor can be described in terms of a simple linear model, as follows:

$$r_i = \sum_{j=1}^{n} \left(a_{ij} f_i + e_i \right)$$

r_i = the reflectance of a given pixel in the ith of m spectral band

n = the number of mixture component (number of endmembers in this pixel)

f_i = the jth of fractional component (proportion of endmember j)

a_{ij} = the reflectance of endmember j in the spectral band i.

Mixing models are based on the assumption that the landscape is formed from continuously varying proportions

of idealized types of land cover with pure spectra, called endmembers. Endmembers are features recognizable in the scene as being abstractions of land cover materials with uniform properties. The pure spectra of endmembers can be measured in the laboratory, in the field, or extracted from the image itself. In an urban environment, these may include impervious surfaces, vegetation covers, water bodies, and bare soils. Through SMA, the areal fractions of the endmembers are quantified at the sub-pixel level, allowing the inference of the morphological characteristics of an urban landscape in terms of endmember composition. Linear SMA is the process of solving for endmember fractions, assuming that the spectrum measured for each pixel represents a linear combination of endmember spectra that corresponds to the physical mixture of some components on the surface weighted by surface abundance. A spectral mixture of endmembers also has the potential to become nonlinear (i.e., when radiations interact with more than one component). Although nonlinear mixing can become significant for some types of analysis, the effects of multiple scattering in the majority of applications are assumed to be negligible. An overview of a simple SMA model workflow is shown in the Figure (1). The analysis begins with the selection of a set of endmembers, followed by applying an SMA model in order to estimate endmember fractions. A good model is one that produces physically realistic fractions (i.e., between 0% and 100%) and measures of error less than a certain threshold (e.g., RMS < 5 DN). That may not happen if the model uses an improper set of endmembers (e.g., the exclusion of an endmember which is represented in the scene, or the addition of an endmember which is not represented). In this case, the selection of endmembers must be refined. This process is repeated until the optimum set of endmembers is identified. Finally, a direct analysis of the fractions or classification is conducted according to the purpose of the application.

4. Material and Methods

The SMA approach is applied on a Hyperion image acquired for the central region of Cairo, Egypt. This section describes the practical steps that are implemented to produce abundance images.

4.1. Study Area

An urban area located in the central area of Greater Cairo has been selected as the area of the study. The upper left and lower right coordinates of the box bounding the study area are 30° 6’ 0.66” N, 31° 8’ 48.77” E and 30° 1’ 35.33” N, 31° 14’ 21.81” E respectively (northing of 3,365,000, easting of 309,000 and northing of 3,309,000, easting of 350,000 meters respectively). The date of acquisition of the Hyperion scene is April 2009 (See Figure (2)).

4.2. Data pre-processing

To prepare the image for the analysis, we performed a number of pre-processing operations following a procedure described in Beck (2003). The first step in this procedure was to convert Hyperion Level 1-B data into absolute radiance using the Band Math function in ENVI software. The second step was to correct the radiance data for atmospheric effects to create reflectance values for the imagery. For this second step, we used the Fast Line-of-sight Atmospheric Analysis of Spectral Hypercube (FLAASH) algorithm in ENVI software. The outcome of this second step was further examined and 38 resulting bands were identified as “bad bands”. This screening left us with only 158 bands (from 0.4268 μ to 2.3352 μ) that we used in the all subsequent analyses performed in this study.

The final pre-processing step applied to the imagery was geometric correction. The Hyperion image was geo-referenced using a geometrically corrected QuickBird high resolution image (0.6 m) of the same study sites, along with some additional ground control points measured by GPS. The number of ground control points is 20. The resulting RMS after the georeferencing process is 3.8 meters.

4.3. Endmembers Selection

Endmembers are selected by determining the Pixel Purity Index (PPI) method. In this study The Pixel Purity Index (PPI) approach is used to help identify the endmembers and find the most spectrally pure (extreme) pixels in hyperspectral data. The Pixel Purity Index (PPI) has been widely used in hyperspectral image analysis for endmembers extraction due to its publicity and availability in different remote sensing packages (Chang, 2006).

The PPI is computed by repeatedly projecting n-D scatter plots on a random unit vector. Extreme pixels in each projection (those pixels that fall onto the ends of the unit vector) are recorded along with the total number of times each pixel is marked as extreme. A Pixel Purity Image is created where each pixel value corresponds to the number of times that a pixel was recorded as extreme.

The determined pure pixel helps to identify the needed endmembers within the Hyperion image.

The process of endmembers selection using PPI can be summarized in the following steps:

i. Run the PPI on ENVI software using 10,000 for the Number of Iterations, and 5 for the Threshold Factor. The "Number of Iterations" parameter refers to the number of n-dimensional projections the PPI algorithm will perform. The "Threshold Factor" parameter is the maximum number of vertexes or extreme pixels that will be considered pure in a given PPI iteration; the value of 5 means that the first five pixels found on a given node of the pixel cloud will be assigned a PPI score of 1. If they are found on a second iteration, then they are assigned a score of 2 and so on. We should notice here that there is no rule of thumb for how many iterations the PPI algorithm needs to run. The number depends on how many bands that image has, the speed of the computer processor, and available memory.
   Once run, the PPI algorithm will yield a "PPI image" showing the number and location of pure pixels, and a "PPI plot" showing the number of iterations performed on the X-axis versus the number of pure pixels found on the Y-axis. The curve shown in the plot can be used to judge whether the number of selected iterations is sufficient. When the curve is flattened (i.e., parallel to the X-axis), this implies that the number of iterations selected for the PPI algorithm is sufficient. When it is not, that is an indication that the PPI algorithm should be executed for more iterations. The PPI image shows the pixels which the PPI identified as pure. The value associated with each pixel refers to the number of times a pixel is identified as pure. For example, if a pixel value is 130, this means that the pixel has been found as extreme 130 times out of 10,000 iterations run by the PPI algorithm.
ii. Select from the resulting PPI image a subset of pixels that can later on be used to derive endmembers. To do so, we first need to identify a cutoff PPI value for the pixels that we want to further consider in our analysis. The cutoff value needs to be big enough to ensure that the pixel was not identified as extreme by chance and that it is representative of an actual endmember. In this study we selected a cutoff value of 10, which means that a pixel needs to be identified as extreme more than 10 times in order to be considered in the image endmember selection. The selection of this cutoff value was somewhat arbitrary to avoid "noise" pixels that are located on the edge of the image.
iii. View the results from Step 2 using the "N-Dimensional Visualizer" tool in ENVI software to identify clusters of pure pixels and derive the final set of endmember candidates from these clusters. The identification of clusters requires good knowledge of the study scene and an iterative process of selection/validation until the clusters of candidate endmembers are identified in the n-dimensional space.
iv. Calculate the average spectral response of the final selected clusters to derive the spectral profiles of candidate endmembers

4.4. Applying linear spectral unmixing

After determining the endmembers, the linear spectral unmixing algorithm was used, which produced a multiband image in which the abundance fractions of each endmember are represented as a single band. The resultant multiband image included an additional Root Mean Square Error (RMSE) band, where the value in each pixel represents the RMSE that resulted from solving for the unmixing algorithm using the endmembers at this particular pixel.

4.5. Accuracy Assessment

An accuracy assessment of the results was performed by superimposing the Hyperion image and the classified QuickBird image, where each pixel of Hyperion data contains 2500 (50 × 50) pixels of QuickBird image. The QuickBird image was classified into 10 classes (land covers) matching the 10 endmembers selected for the Hyperion image. The classified QuickBird image was considered as guidance for assessing the correctness of the abundance fractions. We have randomly selected 40 regions of interest (ROIs) in the Hyperion data (see Figure (3)). Each ROI is located within one pixel of the Hyperion image. To calculate the QuickBird fractions we looped through each of the ROI regions and located the corresponding 2500 QuickBird classified pixels, and these 2500 pixels were examined against each class to determine the number of pixels allocated for this class. Then the fractions were calculated.

The abundance fractions within this Hyperion pixel were then regressed against the endmember (materials) percentages within the corresponding 2500 QuickBird pixels.

Finally, a regression line is created between the Hyperion fractions and QuickBird fractions for each endmember to assess the accuracy of the model.

5. Results and Discussion

5.1. Endmembers Selection Results

Ten endmembers resulted from the PPI process: water bodies (mainly the Nile river), shadow (of the buildings and trees), bare soil (sport yards, dirt in vacant land and farmlands), impervious surfaces (building roofs and roads), and vegetation (croplands and parks) (see Table 1).

Figure (4) below shows the final set of candidate endmembers we derived for this study following the aforementioned procedure.

The final endmember library was selected based on the criteria described above and consisted of 10 endmembers. The number of endmembers per generalized class was as follows: green vegetation—three image endmembers), soil—two image endmembers, and impervious—2 image endmembers. Over 42% of the non-water pixels in the study area were modeled by two endmember models, while an additional 58% of non-water pixels were modeled by three-endmember models.

5.2. Spectral Mixture Analysis Results

The final product of our analysis was a set of fractional abundance maps for each class of materials (i.e. vegetation, impervious surfaces, soil, and water).

Maps of the generalized fractions are shown in Figure (5). Bright areas represent higher fractions and dark areas lower fractions, while black pixels indicate that the material is not present. The oldest part of the city has a mix combination of impervious, vegetation and soil and that is due to the built-up materials used within this area. Major roads are highlighted on the impervious map. Water bodies (River Nile) are highlighted on the left side of the water bodies map. The distribution of the soil fraction is much spottier than the vegetation and impervious fractions. Bare soil tends to be most prominent in areas undergoing construction and expansion, such as the area in the central portion of the soil map.

5.3. Accuracy Assessment Results

After applying the sampling process, a regression line is created between the Hyperion fractions and QuickBird fractions to assess the accuracy of the classification process. Table 2 illustrates the slope, interception, and R^2 values for each generalized endmember.

The average of R^2 is 0.833, which means that the models are averagely fitting around 83% of the data. However, this regression value is mainly dependent on the accuracy of the superimposing process of both the Hyperion data and QuickBird data. Some discrepancies are noted, and this occurs for two reasons: 1) the resolution mismatch between the Hyperion data and QuickBird data, and 2) the accuracy of the ground control points obtained and resulting RMSE values with the rectification process.

The graphs in Figure (6) illustrate the regression results between the Hyperion fractions and QuickBird fractions.

6. Conclusion

In this paper, we have presented: a) an application of spectral mixture analysis in an urban environment using regionally specific endmembers to map the physical abundance of generalized urban materials; b) accuracy assessment for fraction images corresponding to each physical component by comparing these fractions with high resolution image fractions (QuickBird). The area of the study was the central region of Cairo, Egypt. These techniques adequately characterized the diversity of materials that compose land cover within a diverse urban area, and at the same time provided a conceptual structure for grouping the specific materials into three general classes—vegetation, impervious, and soil. These generalized classes can characterize urban land cover regardless of specific construction materials or local environmental variation (Ridd, 1995), facilitating comparison of urban data sets on a global scale. Future research directions include constructing valid spectral references libraries in Egypt for different land covers. Another future development area could be applying SMA in different regions in Egypt, especially the Delta region, which is mainly an agricultural area. We think that creating a spectral library for different crops in the Delta region is a mandatory step for better inventory of crops wealth in Egypt.

References

Beck, R. (2003). EO-1 User Guide, Version 2.3. In. Cincinnati, Ohio: Prepared for Satellite Systems Branch USGS Earth Resources Observation Systems Data Center (EDC).

Chang, C., Plaza, A. (2006). A Fast Iterative Algorithm for Implementation of Pixel Purity Index. *IEEE Geoscience and Remote Sensing Letters, 3*, 1.

Clark, R. N. (1999). *Spectroscopy of rocks and minerals, and principles of spectroscopy, Manual of Remote Sensing,* 3rd ed. New York: John Wiley and Sons (Chapter 1).

Bearman, G. H. (2000). *Spectral imaging: Instrumentation, applications and analysis*. SPIE Publications.

Goetz, A. F. H. (1992). *Imaging spectrometry for earth remote sensing, Imaging Spectroscopy: Fundamentals and Prospective Applications*. ECSC, EEC, EAEC, Brussels and Luxembourg, Netherlands, 1-19.

Leitner, R., Mairer, H., & Kercek, A. (2003). Real-time classification of polymers with nir spectral imaging and blob analysis. *Real Time Imaging*, *9*(4), 245–251.

Ridd, M. K. (1995). Exploring a V–I–S (vegetation–impervious surface–soil) model for urban ecosystem analysis through remote sensing: comparative anatomy for cities. *International Journal of Remote Sensing, 16*, 2165−2185.

Waleed Effat is a GIS Technical Consultant at ESRI Northeast Africa, Egypt since 2005. He is a Ph.D. student at the Faculty of Computers and Information, Cairo University, Egypt from 2010 till the present. His major fields of study are geographical information systems and remote sensing.

Osman Mohamed Hegazy is Professor of Information (Data Engineering) since 1992 at Information Systems, Cairo University, Egypt. He has a Bachelor degree in Electronic Engineering, Faculty of Engineering, Cairo University, Egypt, 1964; Ph.D. in Computer Engineering, University of Leicester, England, 1977. His major fields of study are data engineering, cloud computing and the computer/ human interface.

Mohamed NourEldien is an Associate Professor at Information Systems, Faculty of Computers and Information, Cairo University, Egypt since 2002. He has a Ph.D. in GIS and Information systems from Louis Pasteur University, France, 2001.His major fields of study are geographical information systems, data mining, ecommerce and e-business.

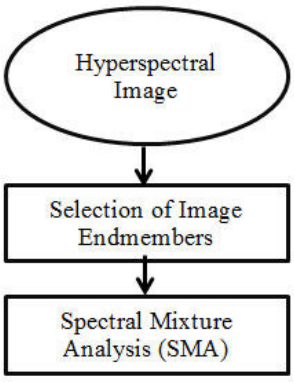

Figure 1: The workflow for applying SMA on a hyperspectral image

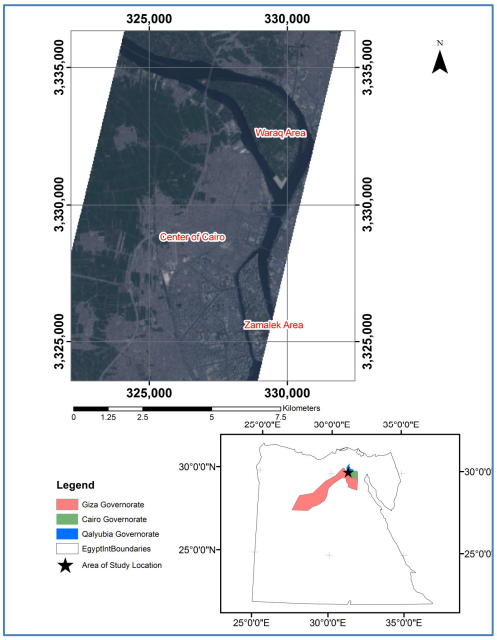

Figure 2: Hyperion image of the area of study and its location with respect to Egypt's international boundaries

Figure 3: Sample from selected ground control points (red crosses)

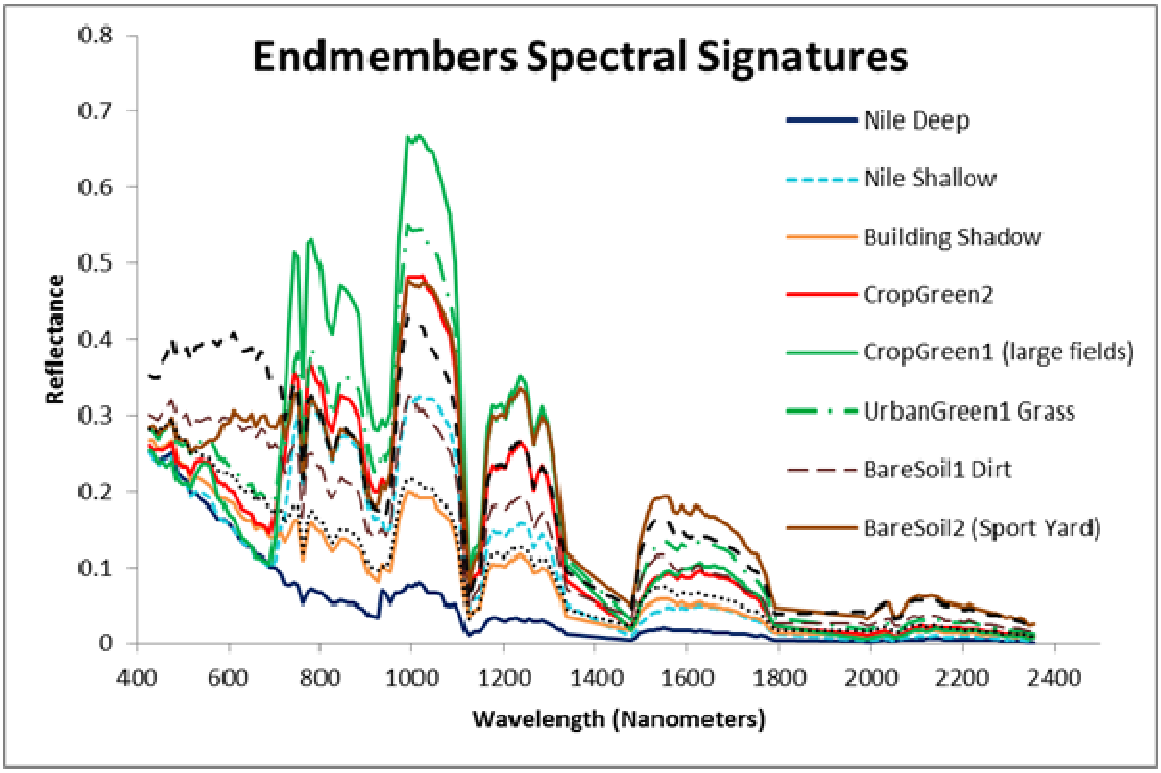

Figure 4: Spectral profile of the extracted endmembers

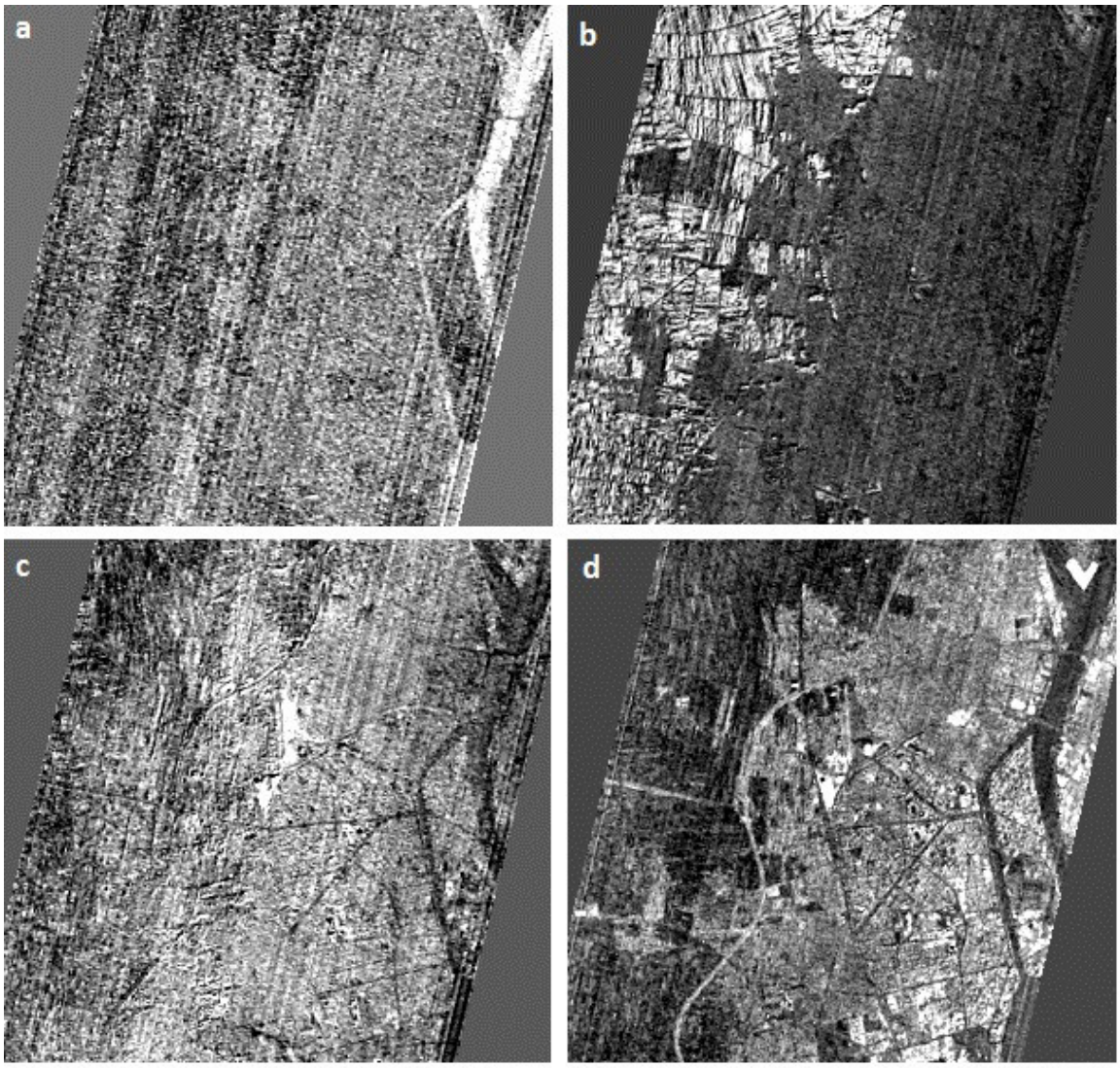

Figure 5: Fraction images produced by the 4-endmember model utilizing vegetation, impervious, dark soil, and water bodies. Brighter areas indicate higher abundance while darker areas indicate lower abundance

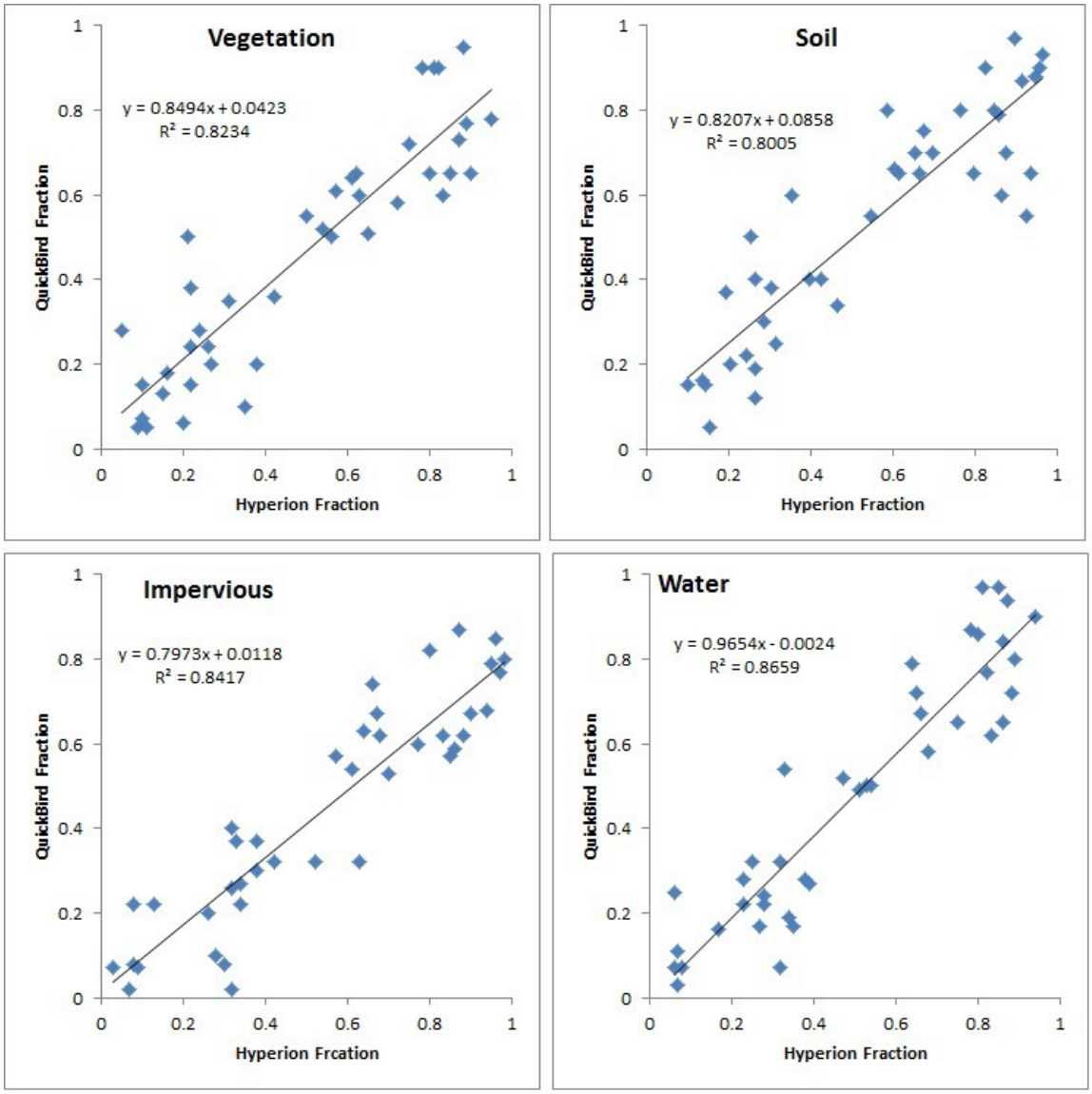

Figure 6: Regression line between Hyperion fractions and QuickBird fractions for each generalized endmember

Table 1. List of Extracted Endmembers

Index	Endmember Name	Description
1	Nile Deep	The deep area in the Nile River
2	Nile Shallow	The shallow area in the Nile River
3	Building Shadow	The shadow of the buildings within the area of the study
4	CropGreen2	Medium sized crop fields mainly including some vegetables crops
5	CropGreen1 (large fields)	Large sized crop fields mainly including wheat and cotton crops
6	UrbanGreen1 Grass	Green areas within residential areas (parks)
7	BareSoil1 Dirt	Lands that are ready to be cultivated with no vegetation.
8	BareSoil2 (Sport Yard)	Sport yard areas
9	Built HighAlbedo (Concrete)	Concrete structures and newly paved roads
10	Built LowAlbedo (OldRoads)	Old roads

This table lists the extracted endmembers and provides a full description for each endmember.

Table 2: Regression outputs: Slope, interception, and R2 values for each endmember

Endmember	**Slope**	**Interception**	**R^2**
Vegetation	0.849	4.2%	0.823
Soil	0.821	8.6%	0.800
Impervious	0.797	1.2%	0.842
Water	0.965	0.24%	0.866